Journal Pre-proof

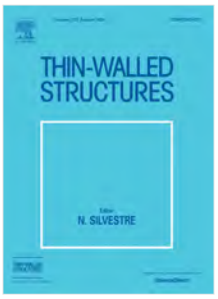

Experimental nonlinear response of a new tensairity structure under cyclic loading

Stefano Catarci, Sawan Kumar Guruva, Biagio Carboni,
Giuseppe Quaranta, Walter Lacarbonara

PII: S0263-8231(24)00605-0
DOI: https://doi.org/10.1016/j.tws.2024.112163
Reference: TWST 112163

To appear in: *Thin-Walled Structures*

Received date : 15 February 2024
Revised date : 16 June 2024
Accepted date : 25 June 2024

Please cite this article as: S. Catarci, S.K. Guruva, B. Carboni et al., Experimental nonlinear response of a new tensairity structure under cyclic loading, *Thin-Walled Structures* (2024), doi: https://doi.org/10.1016/j.tws.2024.112163.

Experimental nonlinear response of a new tensairity structure under cyclic loading

Stefano Catarci, Sawan Kumar Guruva, Biagio Carboni, Giuseppe Quaranta, Walter Lacarbonara

Department of Structural and Geotechnical Engineering, Sapienza University of Rome, Via Eudossiana 18, 00184 Rome, Italy

Abstract

Pneumatic structures are recognized as promising thin-walled structures for their advantageous features such as lightness, portability, versatile design, and ease of installation. Although their bearing capacity under monotonic static loads can be formidable, their inherent dissipation capacity is low and thus entails significant limitations when counteracting dynamic loads. A novel tensairity structure is here proposed to overcome this drawback. The innovative design features a cylindrical inflatable element integrated with NiTiNOL cables wrapped around and affixed to a slender beam positioned along its generatrix. A laboratory-scale prototype is employed to assess how the structure behaves under cyclic loading in comparison to a standalone inflated beam and a conventional tensairity structure outfitted with steel cables. This experimental study delves into the influence of internal pressure and pretension levels of the metallic cables. Experimental results unfold a smooth softening-type hysteretic behavior under cyclic loading, which is accompanied by a slight stiffness degradation and a moderate pinching. The comparative analysis of the experimental results also demonstrates the substantially improved and consistent dissipation capacity of the presented novel concept of tensairity structure, which thus offers superior stability under cyclic loads. A parametric identification based on a modified Bouc-Wen model is finally performed to simulate the hysteretic response of the structure. A correlation is also established between the identified parameters of the phenomenological model and the internal pressure, type and cables pretension levels. The excellent agreement between numerical predictions and experimental force-displacement cycles other than those used for the parametric identification demonstrates the suitability of the adopted phenomenological modeling.

Keywords: Inflatable structure, Lightweight structure, Damping, Hysteresis, Identification, NiTiNOL, Shape memory alloy, Tensairity.

1. Introduction

Advanced materials and innovative manufacturing technologies make lightweight structures more and more attractive for a wide range of applications in aerospace and civil engineering because a significant load capacity can be attained while ensuring low weight, compact transport volume, versatile design and simple erection process [1, 2]. Within this framework, the use of pneumatic structures (i.e., insufflated, aspirated and inflated structures) has been largely explored in the past decades starting from the initial works proposed at the beginning of the 20th century [3]. The first proposal of pneumatic structures is due to Frederick W. Lanchester, who patented in 1919 an insufflated dome for campaign hospitals [4]. Soon after, in 1929 Kaneshige Nohmura developed air-inflated membrane tents where rigid arches and masts were replaced by inflated tubes. The interest towards pneumatic structures has raised significantly since the fifties. This rising interest was stimulated by the development of new lightweight materials and a few strategic applications, including air-supported radomes to protect radars in United States [5] and an aerospace inflatable structure within Echo 1 mission [6].

Most of the existing studies on inflatable pneumatic structures aim at understanding and enhancing their behavior under monotonic static loading conditions, with special attention about the occurrence of instability phenomena. In fact, since modern fabrics and joints can sustain relatively high tension levels, inflatable structures can withstand significant static loads without experiencing excessively large displacements thanks to the low compliance that can be ensured by the internal pressure. However, wrinkling phenomena can occur in the inflated membrane once its pretension level due to internal pressure is exceeded by compression stresses. This issue has been addressed by theoretical studies into the behavior of inflatable structures [7–10], while experimental investigations have been conducted more recently and are still ongoing. For instance, Main et al. [11] investigated the static response of inflatable fabric beams for aerospace applications. They developed and validated experimentally a bending model for inflatable beams starting from basic assumptions about the state of stress in the fabric. So doing, Main et al. [11] demonstrated that the bending behavior of inflatable fabric beams is identical to that of conventional solid elastic beams provided that the beam fabric remains unwrinkled. Wielgosz and Thomas [12] presented an experimental and analytical study about the deflection of inflatable fabric panels at high internal pressure levels under static load. They developed a new inflatable beam model and then derived the wrinkling loads from equilibrium equations. Wang and Tan [13] proposed the use of shape memory alloy (SMA) wires in order to control wrinkling phenomena due to an applied static load. They proposed to attach SMA wires to the stretched side of the inflated beams (i.e., the side opposite to the wrinkled/compressed region), which are then electrically

activated in order to generate the recovery force required to remove the wrinkles in the inflated membrane. Experimental tests on a prototype structure show that this active strategy is able to improve the overall bending performance of inflated beams. A different (passive) strategy against wrinkling of inflated beams and arches was instead presented by Brayley et al. [14], making use of external reinforcing straps to control the membrane instability. Their large-scale experimental bending tests demonstrated that the straps increase the post-wrinkling capacity of inflated structures.

In view of a possible European design code dedicated to tensile textile structures, Thomas and Bloch [15] presented numerical simulations and experimental data to support the definition of serviceability and ultimate limit states for airbeams/airarches under static loads in terms of maximum displacement, wrinkle onset and wrinkle-induced collapse. Experimental dynamic characterization of inflatable structures has received less attention compared to static tests. For example, dynamic tests performed by Slade et al. [16] have shown that the modal features of inflatable structures is sensitive to the surrounding environmental conditions (i.e., atmospheric and vacuum condition). Park et al. [17, 18] identified mode shapes and natural frequencies of an inflatable torus structure by means of piezoelectric patches non-intrusively integrated into the membrane. Lew et al. [19] identified natural frequencies and damping ratios of an inflatable torus under different temperatures, and quantified the related uncertainties.

Within the framework of inflatable constructions, tensairity structures are a relatively new concept [20]. In its basic configuration, a tensairity structure combines an airbeam with a slender strut fixed on its external surface, along with a pair of cables wrapped around the pneumatic element and connected at the ends of the strut. When the tensairity experiences transverse loading on the strut, tension forces arise in the cables and these, in turn, are absorbed by the rigid strut as compressive forces. This distribution enhances the load bearing capacity and the lateral stiffness provided to the strut avoids instability phenomena. For instance, Luchsinger and Galliot [21] and Luchsinger et al. [22] performed numerical and experimental studies about symmetric and non-symmetric spindle-shaped tensairity girders, respectively, under bending. Numerical and experimental results about spindle-shaped tensairity columns under static axial loads have been presented by Plagianakos et al. [23], while Wever et al. [24] investigated the beneficial effect of fabric webs on their capacity. Two novel configurations for spindle-shaped tensairity girders have been proposed by Galliot and Luchsinger [25]: while a continuous coated-fabric web is inserted into the airbeam in the first configuration, the second configuration employs a discrete reinforcement consisting of multiple steel wire ropes. Numerical and experimental studies about tensairity structures with curved geometries have been also proposed, such as tensairity arches [26, 27] and domes [28–30]. Vernarsky et al. [31] developed a computational fluid

dynamics model to study the response of cylindrical tensairity beams subjected to wind loads. The only available experimental research about the dynamics of tensairity structures has been presented by Klis et al. [32], who performed a complete linear modal identification of a spindle-shaped tensairity beam for different internal pressures.

Although tensairity structures are a relatively novel concept, some applications have already been reported in the literature. Almost all existing applications deal with (permanent or ephemeral) civil constructions, such as a reduced-scale prototype of roadway bridge with 8 m span and 3.5 tons maximal load [33], the roof of a parking garage [33], a skier bridge with 52 m span [34], and temporary pavilions [35]. Breuer and Luchsinger [36] also presented the proof-of-concept of a tensairity kite. Some novel concepts based on tensairity structures are also emerging. For example, Cao et al. [37] introduced the concept of tensairity truss, where a spindle-shaped airbeam is coupled with cables and a truss element.

This overview about the existing studies on tensairity structures shows that significant advances have been made to understand their behavior and enhance their performance under monotonic static loading. Conversely, there is no information about their response under cyclic loading. Another aspect that has been overlooked so far is the improvement of their energy dissipation capacity. Actually, as the demand for lighter constructions is growing, the energy dissipation capacity in tensairity structures is likely a more critical design factor than the bearing load capacity for several applications. In this regard, the role of the internal pressure of an inflated structure can be a crucial design problem. While an increase in internal pressure proves advantageous for enhancing the load-bearing capacity and stiffness of inflated structures, experimental evidence suggests that this may compromise their energy dissipation capacity [38].

The present work aims to advance our understanding of tensairity structures with a focus on their behavior under cyclic loading. To this end, a new concept of tensairity structure is presented. This novel design incorporates a cylindrical inflatable component coupled with NiTiNOL cables wrapped around and attached to a slender beam aligned along its generatrix. At the ends of the slender beam, pneumatic and manual mechanisms are positioned to adjust the tension levels of the cables. A laboratory-scale prototype of this new structural system was built to investigate and characterize its behavior under cyclic loading through extensive experimental tests. This experimental investigation explores the influence of internal pressure and the cables pretension levels. It also allows to compare the overall stiffness and dissipation capacity of this innovative tensairity system with those of both the inflated beam alone and a conventional tensairity structure equipped with steel cables. Finally, the parametric identification of a modified Bouc-Wen model is performed to describe the experimental response of the structure. The identified model

parameters are then correlated with internal pressure, cable type, and pretension levels. The very good agreement between numerical predictions and experimental force-displacement cycles confirms the accuracy of the adopted phenomenological modeling.

2. Prototype of the new tensairity structure

This research deals with a new concept of tensairity structure seeking to achieve a better dissipation capacity. This tensairity structure consists of a cylindrical inflatable element and NiTiNOL cables wrapped around and affixed to the ends of a slender beam positioned along its generatrix. Figure 1 shows the designed layout of the laboratory-scale prototype developed to evaluate its behavior under cyclic loading. The top picture shows a plane view of the tensairity structure with the pneumatic element, the wire rope, the strut equipped with control mechanisms at the ends, and the two bearings securing a simply-supported layout. Close-ups of pneumatic and pretensioning control systems are given in the smaller pictures. The pneumatic system is constituted by a pulley mounted on a linear sliding mechanism. The pneumatic actuator is fixed to the strut by means of a steel angular connection and its shaft can displace the pulley around which the rope is wrapped. The manual pretensioning mechanism is composed by a steel hollow box, mounted on a linear guide, which can be displaced by screwing a nut positioned on a bolt passing through the box. The bolt is also fixed to one end of the strut by means of another angular steel connection. It is noted that this prototype also allows to test the inflated beam alone and a conventional tensairity structure outfitted with steel cables.

The cylindrical inflatable element is made of a polyethylene (Hypalon) sheet with a thickness of 0.6 mm whereas its span and diameter are equal to 1.8 m and 0.15 m, respectively. It consists of PVC fabric with orthotropic properties, with the stronger direction arranged along the transverse direction of the cylinder, reflecting the presence of larger circumferential stress induced by inflation compared to the longitudinal direction. The thin beam acting as strut of the tensairity is made of aluminum and is hosted within a pocket arranged along the generatrix of the cylindrical inflatable element. Such aluminum beam has a rectangular cross-section with width and thickness being 50 mm and 6 mm, respectively, and its length 2 m. It is observed that the length of the strut exceeds the span of the cylindrical inflatable element, effectively constraining the structure and ensuring the stability of its control systems. Hence, each end of the strut is fixed to a circular ring, which, in turn, is connected to a support fixed to the ground. The metallic cables that act as ties of the tensairity have a circular cross-section with a diameter of 0.6 mm. This laboratory-scale prototype shown in Fig. 2 features two control systems at the two ends. On one side, there is a control

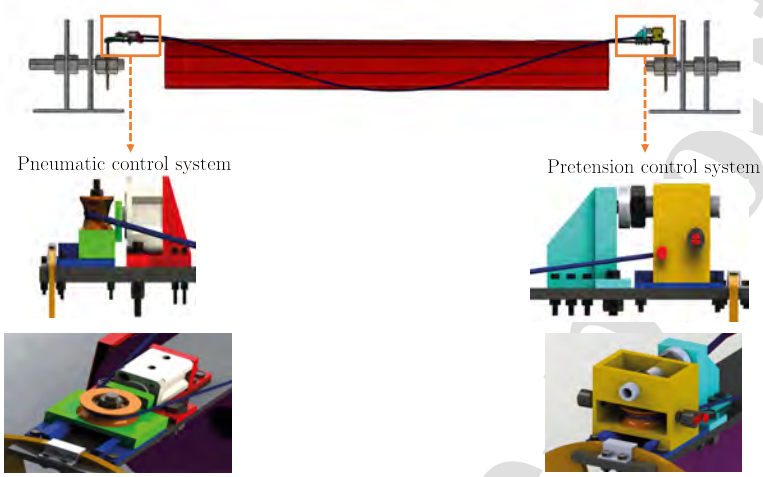

Figure 1: Layout of the tensairity prototype. The top picture shows the inflatable element, rope, strut, control mechanisms and supports. Details of pneumatic and pretensioning control systems are given in the close-ups on the bottom.

system that provides the cables pretension. The internal air pressure control system is fixed at the other end, and it also includes a manometer. Two dovetail guided rails with length equal to 50 mm are screwed along the edges of the strut to facilitate the installation of the control systems while ensuring a smooth sliding.

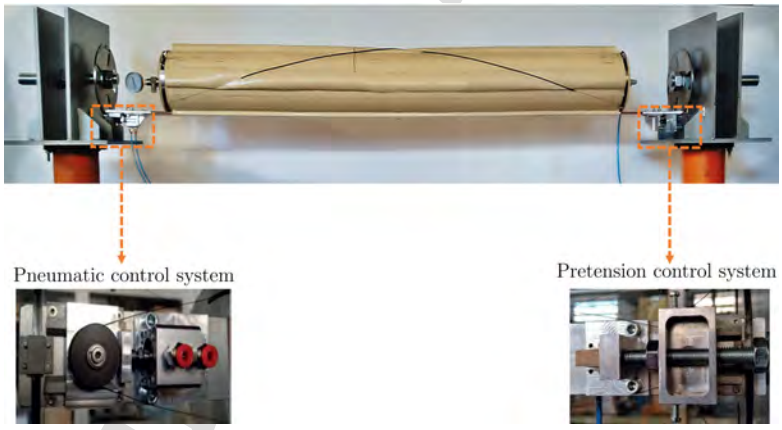

Figure 2: Laboratory prototype of the tensairity: overall view together with details of the pneumatic and pretension control systems.

The stress-strain relationships of the baseline materials obtained from tensile tests performed by means of

a Zwick-Roell Electrostatic Test Machine are plotted in Fig. 3. The specimen length was 150 mm for steel and NiTiNOL cables, while a sample 250 mm long and 40 mm wide was employed for Hypalon. Tensile cyclic tests were carried out to evaluate the material hysteresis under cyclic loading and to characterize the austenite-martensite transition of NiTiNOL. The tests were performed by estimating the elongation of the specimens as the ratio between the applied displacement and the initial length. This simplified approach, in which the strains are not directly measured on the specimens, is justified by the small restoring forces provided by the samples relative to the full load capacity of the employed cell (10 kN). In this condition, the deformability of the cell, compared to that of the specimens, is negligible. The cyclic response of the Hypalon strip subjected to a uniaxial tension history applied in displacement control is shown in Fig. 3 (a). The first loading branch up to a strain amplitude of 2% shows a softening-hardening behavior. Subsequently, multiple cycles within the strain range $[0.8\%, 2\%]$ were obtained to assess the material dissipation capacity. The material exhibits a tangent elastic modulus of 110 MPa at the strain of 0.03%, which decreases to approximately 83 MPa at a strain of 0.287%. Beyond this point, the material displays a clear hardening, reaching a tangent elastic modulus of 175 MPa at a strain of 1.84%. Considering the last loading-unloading cycle and the associated secant stiffness and internal area, an equivalent damping ratio of 0.66% was estimated across the investigated strain interval. An additional monotonic loading test was conducted to determine the ultimate strain and stress, which were found to be 15.43% and 12.88 MPa, respectively. The maximum tensile stress of the Hypalon membrane has not been measured experimentally. Indeed, the failure is likely governed by adhesive bonding; however, the present experimental campaign was not intended to investigate the behavior of the tensairity close to collapse. Anyway, the (nominal) maximum tensile stress of the Hypalon membrane can be assumed to be about 16 MPa. The maximum tension experienced by the Hypalon membrane in the present experimental campaign corresponds to an internal pressure of 0.3 bar, and it can be roughly estimated equal to $\sigma = pr/t = 3.75$ MPa, where p, r and t indicate pressure, radius and thickness of the cylinder, respectively. Figure 3 (b) portrays the stress-strain behavior of a steel wire under cyclic tensile loads. The material shows an elastic modulus equal to 180 GPa, a yield strain of 1.14%, an ultimate strength of $2,133$ MPa at an axial strain of 1.44%; as expected, it does not exhibit dissipation capacity. Finally, the superelastic cycles of a NiTiNOL wire are reported in Figure 3 (c). Herein, under the simplifying assumption of an isothermal behavior, the following mechanical features were identified: austenitic and martensitic elastic moduli of 56.44 GPa and 42.45 GPa, respectively; start and end of transformation loading stresses equal to 548 MPa and 737 MPa, respectively; start of transformation unloading stress of 595 MPa and total transformation strain of about 5.8%. The use of NiTiNOL with super-elastic properties [e.g., 39–41] instead of classical

steel aims at boosting the energy dissipation of the tensairity under cyclic loading. Shape memory alloys are especially suitable for this goal thanks to their pseudo-elastic behavior, as illustrated in Fig. 3 (c). A significant amount of energy is dissipated when the NiTiNOL cable undergoes a tensile cycle that exceeds a strain of 1.2%, and no residual inelastic strain remains after unloading. This phenomenon can be exploited to enhance dynamic damping in the tensairity structure. Below a threshold strain of about 1.2%, NiTiNOL does not provide dissipation. Therefore, pretensioning of the cable is needed to enable energy dissipation under cyclic loading. According to Fig. 3 (c), the optimal prestress value is approximately 550 MPa, corresponding to the onset of the austenite-martensite phase transformation.

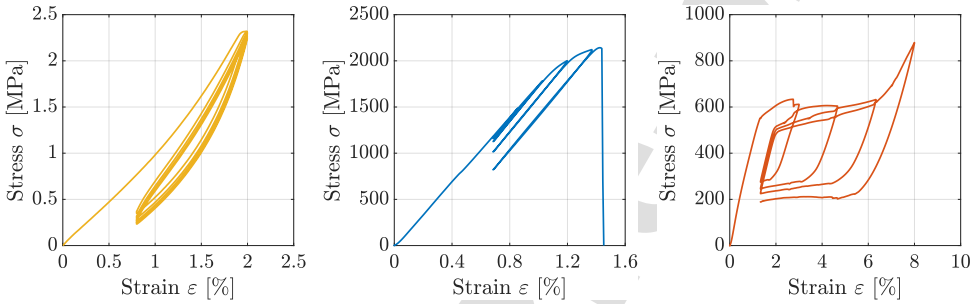

Figure 3: Stress-strain relationships for (a) Hypalon, (b) steel wires, and (c) NiTiNOL wires.

3. Nonlinear behavior of the tensairity under cyclic loading

3.1. Experimental results

Figure 4 depicts the laboratory layout that was utilized to test the inflated structure under cyclic loading. The tensairity is simply-supported at the ends according to the constructed boundary conditions. The ends of the struts are inserted in two slots at the border of two steel rings. Two large bolts are fixed to external supports and pass through the rings, thereby sustaining the tensairity. The assembly of the tensairity involves the following main phases. The slender strut is first inserted into the pocket available on the pneumatic cylinder, which is then inflated up to the target pressure level. The ends of the strut are next placed into their housings within the metal rings, and the two ropes are then wrapped around the inflatable cylinder. They are anchored at the ends and pretensioned in compliance with the target prestress level. Multiple pockets can be observed in Fig. 4 (i.e., four pockets spaced 90° apart from one another). This is because the tensairity has been designed to equip the inflatable cylinder with additional three struts and three pairs of ropes in order to possibly cope with multi-directional loading conditions.

The main test specifications include the internal pressure of the airbeam as well as the type and pre-tensions of the wires. The control mechanisms were employed to set the internal pressure of the pneumatic element and the pretension level of the wires at the beginning of the test. The continuous monitoring of the pressure level by means of the manometer confirmed that its value was almost constant during the test. Unfortunately, direct measurement of the pretension force in the wires was not possible at the time of the test, and thus their shortening is considered to quantify the pretension level. Next, an actuator was placed at the midspan of the beam and a displacement-controlled cyclic loading was applied. In this way, the load can be represented as a point load applied at the midspan. This is accomplished by means of a universal testing machine (MTS Systems Corporation) and an ad hoc connecting frame, see pictures of the tests in Fig. 5. Load levels and midspan displacements experienced by the inflated structure were measured. For each configuration and displacement amplitude, 15 sinusoidal cycles with a frequency of 0.5 Hz were applied using the MTS actuator in displacement control. A load cell was positioned between the rectangular connecting frame and the midspan to measure the restoring force. Both the applied displacement and the restoring force were recorded simultaneously to obtain force-displacement cycles. Subsequently, one cycle was extracted to characterize the structural response.

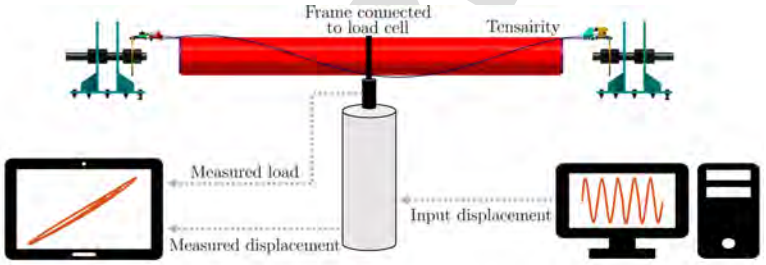

Figure 4: Layout of the laboratory setup for the experimental characterization of the tensairity under cyclic loading.

Figures 6-7 illustrate the cyclic response of the airbeam for different values of the internal pressure p corresponding to various maximum vertical displacements x imposed at the midspan. The internal pressure in Figs. 6-7 is 0.05 bar, 0.10 bar, 0.20 bar, and 0.30 bar whereas the maximum vertical midspan deflection ranges between 5 mm and 35 mm with a constant step of 5 mm. It is noted that the smallest and the largest cyclic loading condition correspond to a maximum displacement-to-span ratios close to 0.3% and 2%, respectively. In particular, Figs. 6-7 show the relationship between the force F and the displacement x for the inflated standalone beam as well as for the tensairity with pretensioned metallic wires made of

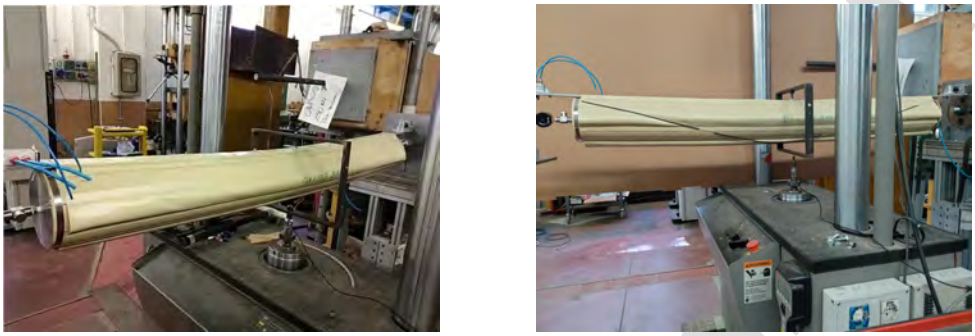

(a) (b)

Figure 5: Experimental testing of the tensairity under cyclic loading: (a) configuration without cables and (b) with NiTiNOL wires.

steel or NiTiNOL. A pretension level corresponding to a wire shortening Δ equal to 10 mm (i.e., minimum pretension level during the test) and 20 mm (i.e., maximum pretension level during the test) is considered in Fig. 6 and Fig. 7, respectively.

Figures 6-7 highlight a smooth softening hysteretic behavior under cyclic loading for all displacement levels. The general shape of the hysteresis loops is preserved, upon varying the main features of the structure (such as internal pressure of the inflated beam, type and pretension level of the wrapping wires). A moderate pinching emerges from the measured force-displacement cycles. In particular, the pinching exhibited to varying degrees in all configurations can be associated with the constitutive behavior of both Hypalon and NiTiNOL (see Fig. 3). Figures 6 and 7 further highlight that there is a slight degradation of the stiffness as function of the maximum displacement for both the standalone inflated beam and the tensairity with steel or NiTiNOL wires. The stiffness gets reduced by about 10% on average when both the standalone inflated beam and the tensairity with steel or NiTiNOL wires are subject to cyclic loading with a maximum displacement level that varies from 5 mm to 35 mm. This degradation can be associated with the boundary conditions implemented for the slender beam, whose ends are free to slightly translate along the direction parallel to the longitudinal axis of the airbeam. Furthermore, it can be inferred that the internal pressure of the inflated beam largely influences the ultimate capacity (i.e., the maximum force measured for an imposed displacement level). For instance, increasing the internal pressure from 0.05 bar to 0.30 bar enhances the ultimate capacity by as much as 40% at the maximum imposed displacement level for both the standalone inflated beam and the tensairity with steel wires no matter what their pretension level is. Such increase of the ultimate capacity as function of the internal pressure is about 46% and 33% for the tensairity with

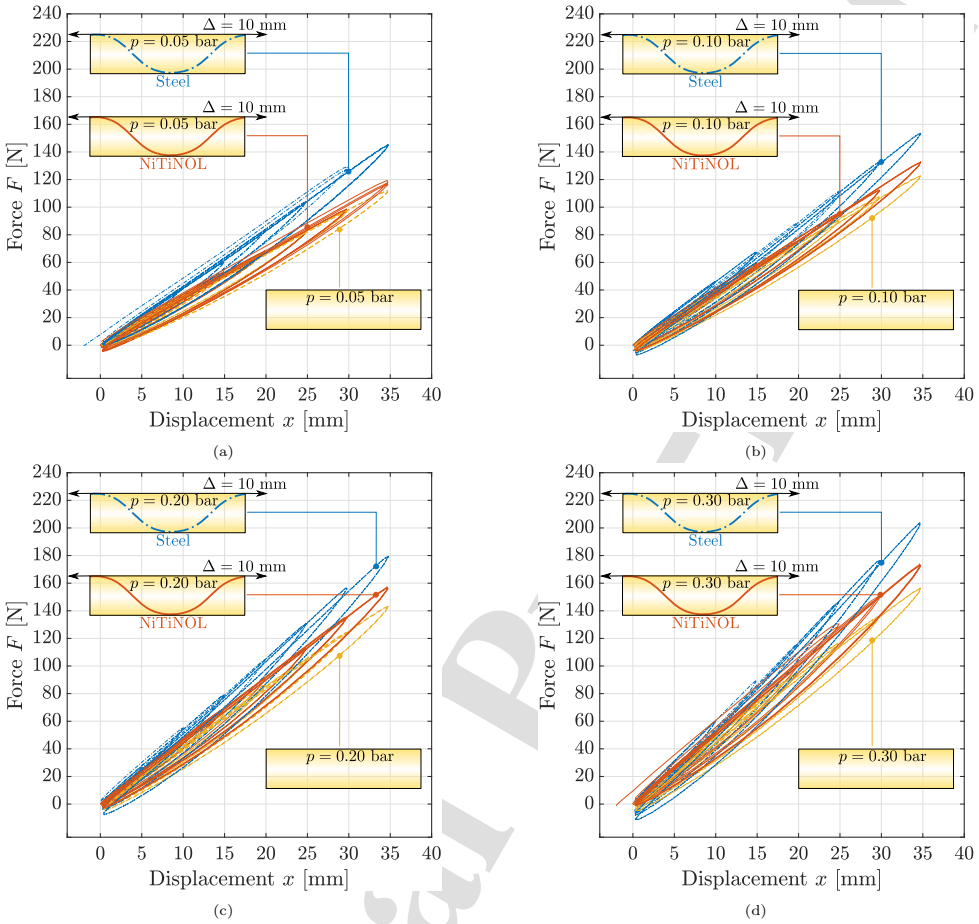

Figure 6: Hysteretic force-displacement cycles for the standalone inflated beam and for the tensairity with metallic wires made of steel or NiTiNOL at the minimum pretension level of 10 mm: the internal pressure of the airbeam is set to (a) 0.05 bar, (b) 0.10 bar, (c) 0.20 bar, and (d) 0.30 bar.

NiTiNOL wires at the minimum and maximum pretension level, respectively.

Figure 8 provides further information about the influence of the wires' material (i.e., steel or NiTiNOL) on the actual stiffness of the tensairity. In fact, Fig. 8 illustrates the normalized stiffness $\bar{K}$, defined as the ratio between the stiffness of the tensairity (with steel or NiTiNOL cables at either minimum or maximum pretension) and the corresponding value of the standalone inflated beam for the corresponding maximum value of the imposed displacement throughout the cyclic loading (the secant stiffness corresponding to the

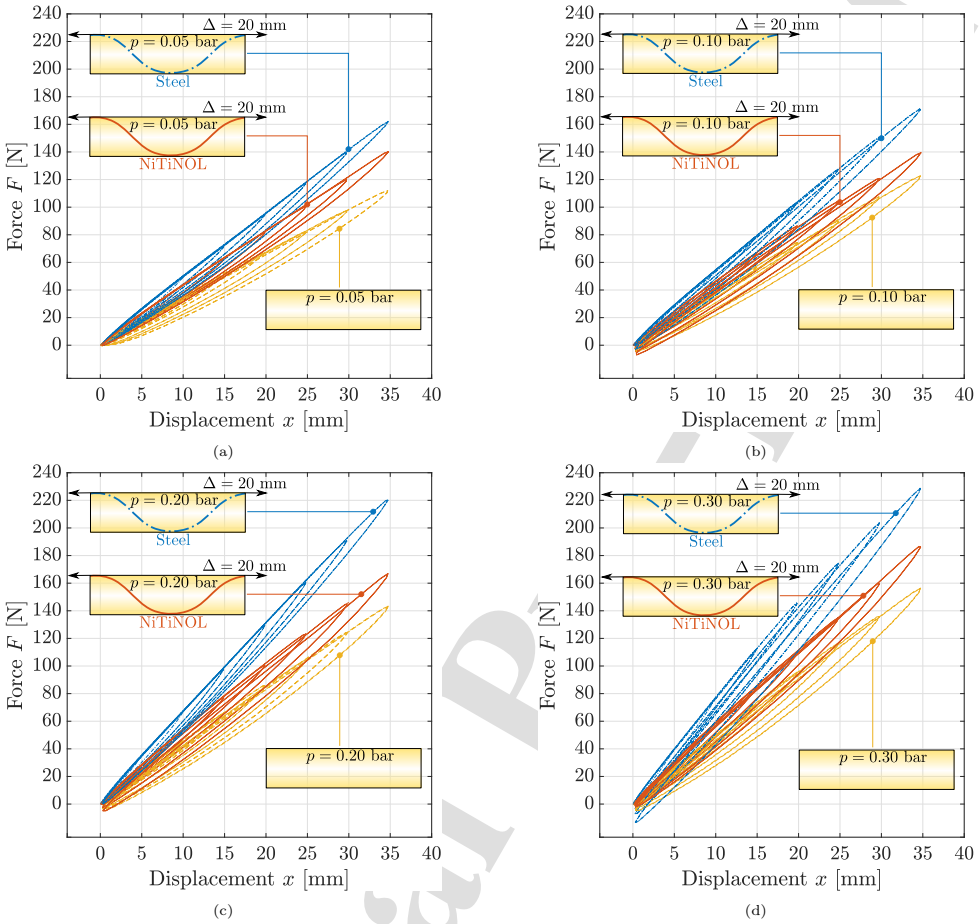

Figure 7: Hysteretic force-displacement cycles for the standalone inflated beam and for the tensairity with metallic wires made of steel or NiTiNOL at the maximum pretension level of 20 mm: the internal pressure of the airbeam is set to (a) 0.05 bar, (b) 0.10 bar, (c) 0.20 bar, and (d) 0.30 bar.

peak displacement is considered).

Figure 8 confirms that wrapping the inflated beam with metallic wires enhances its stiffness. The actual stiffness of the tensairity equipped with steel wires is larger than it would be attained by means of NiTiNOL wires. This is a direct consequence of the elastic modulus, which is larger for steel than for NiTiNOL. Figure 8 shows that the the stiffness increase conferred by the metallic wires is not constant under cyclic loading, but it varies almost linearly with the imposed displacement. It can be observed in Fig. 8 that

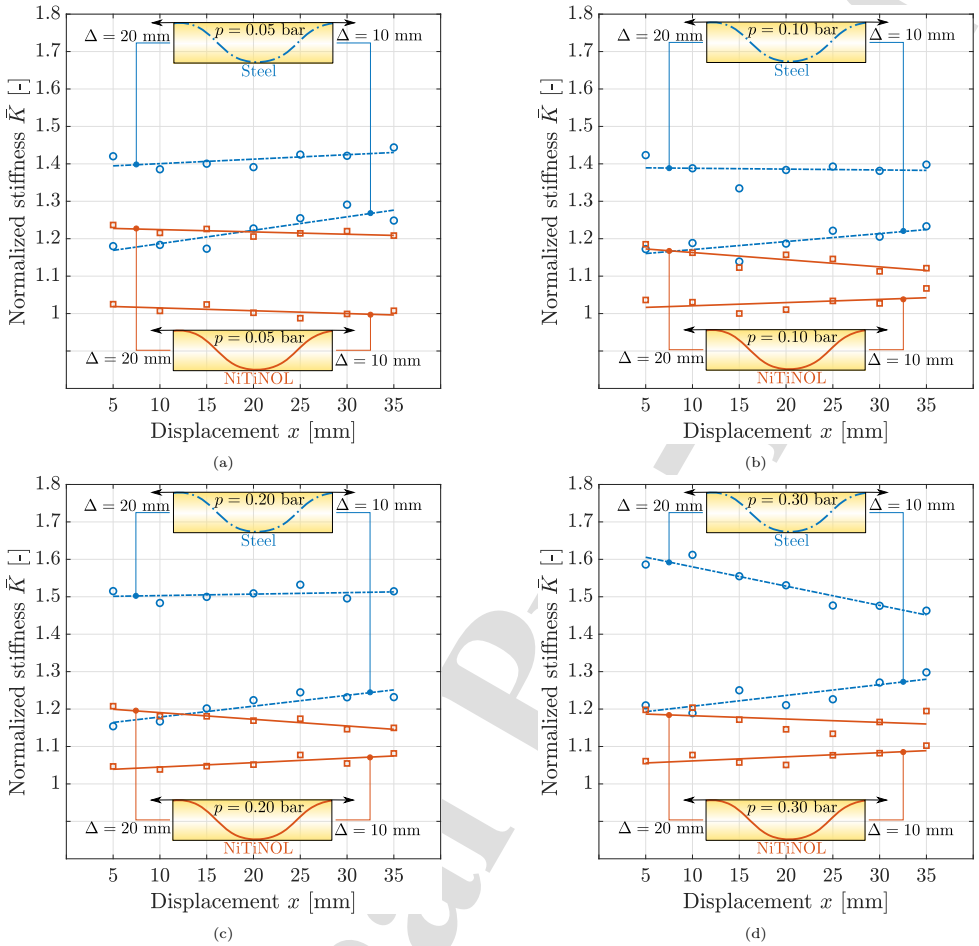

Figure 8: Stiffness of the tensairity with metallic wires made of steel or NiTiNOL normalized with respect to the corresponding value estimated without cables: the internal pressure of the inflated beam is set to (a) 0.05 bar, (b) 0.10 bar, (c) 0.20 bar, and (d) 0.30 bar.

the stiffness augmentation in the inflated beam differs between the two types of wires. This variation is contingent upon the specific combination of factors, including internal pressure, wire material, pretension, and maximum displacement during cyclic loading. On the one hand, steel wires at the minimum pretension level amplify the stiffness of the inflated beam by about 20% on average: in such condition, the stiffness increment is linearly proportional to the increment of the imposed maximum displacement and it is further magnified by increasing the internal pressure. On the other hand, the stiffness amplification attributable to

NiTiNOL wires at the minimum pretension does not exceed 10% and its displacement-dependent variation is limited. The introduction of steel wires under maximum pretension leads to a remarkable amplification of the stiffness of the inflated beam: this increment is approximately 40% if the internal pressure is lower than 0.10 bar whereas it grows up to about 50% on average otherwise. However, while the stiffness increment due to steel wires at the maximum pretension level is almost constant up to a pressure level of 0.20 bar over the considered range of maximum imposed displacements, it suffers a reduction at 0.30 bar of about 60% and 45% at 5 mm and 35 mm, respectively. Wrapping NiTiNOL wires with maximum pretension around the inflated beam increases the stiffness by about 20% on average, thereby resulting less effective than the conventional steel wires outfitting. Such a stiffness increment of the inflated beam due to NiTiNOL wires is not constant, but it slowly decays with the growth of the maximum imposed displacement. Notably, the decay rate of the stiffness amplification due to NiTiNOL wires at the maximum pretension remains low even when the internal pressure is at its highest values, whereas the use of steel wires exhibits a sudden reduction under such conditions.

Figures 9-10 portray the energy dissipation capability under cyclic loading by providing the equivalent damping ratio ξ_{eq} as function of the maximum displacement throughout the cyclic loading. The equivalent damping ratio ξ_{eq} is defined as follows:

$$\xi_{eq} = \frac{W_D}{4\pi W_E}, \tag{1}$$

where W_D represents the area enclosed by the hysteresis loop and W_E denotes the stored energy. In particular, Figs. 9-10 provide the equivalent damping ratios of the tensairity with pretensioned metallic wires made of steel or NiTiNOL at the minimum and maximum pretension levels, respectively, together with those of the standalone inflated beam.

The results of the experimental campaign confirm that increasing internal pressure and wrapping metallic wires are beneficial to improve the stiffness of the inflated beam. At the same time, the experimental results reported in Fig. 9 and Fig. 10 demonstrate that they generally have a negative effect on the dissipation capacity of the structure under cyclic loads. Nevertheless, the airbeam outfitted with NiTiNOL wires demonstrates a greater dissipation capacity compared to the one equipped with steel wires. This finding can be primarily attributed to the distinctive shape of the unloading-reloading cycles in the stress-strain curves of these metallic alloys.

The equivalent damping ratio of the inflated beam alone is approximately 1.05%-1.2% and grows up to 1.4%-1.5% when the imposed peak displacement is 5 mm and 35 mm, respectively. Lower values in these ranges correspond to the maximum internal pressure of the airbeam and vice versa. The tensairity with steel

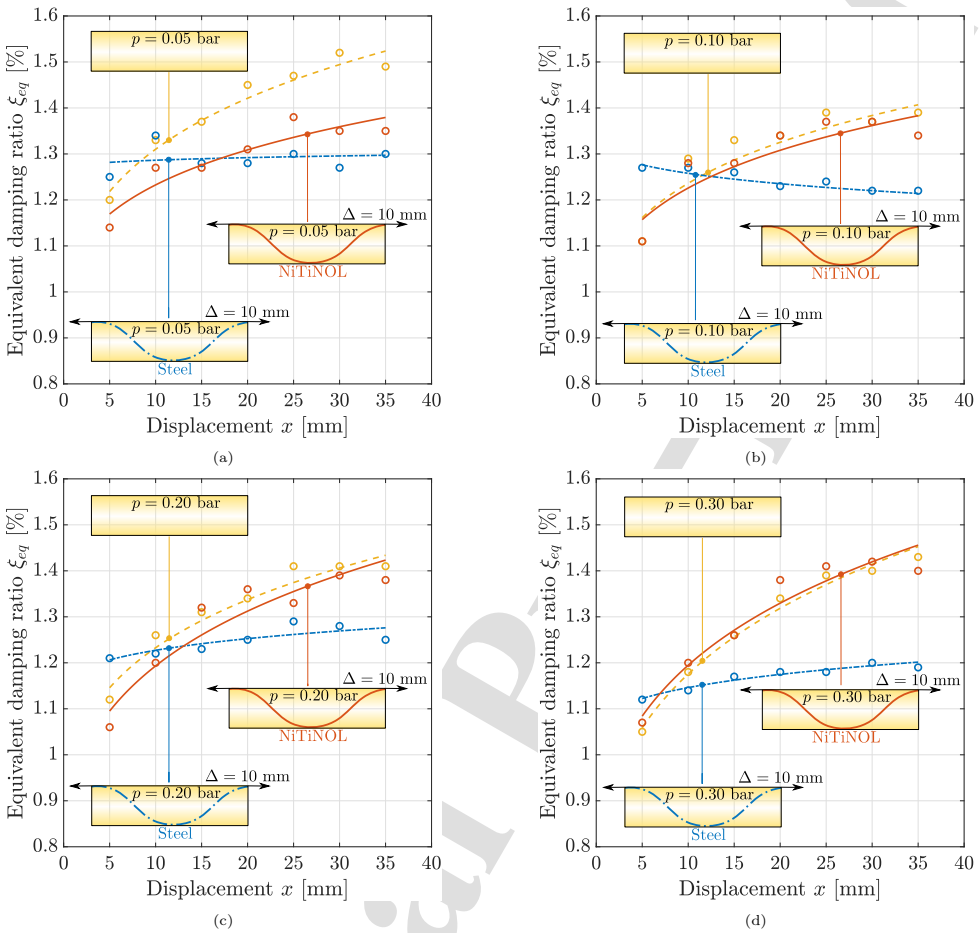

Figure 9: Equivalent damping ratio of the tensairity without cables and with metallic wires made of steel or NiTiNOL at the minimum pretension level of 10 mm: the internal pressure of the inflated beam is set to (a) 0.05 bar, (b) 0.10 bar, (c) 0.20 bar, and (d) 0.30 bar.

wires at the minimum pretension level has an equivalent damping ratio lower than the standalone airbeam for mid-large values of the imposed peak displacement: for instance, it reduces from about 1.3% at 0.05 bar to 1.2% at 0.30 bar when the displacement amplitude is 35 mm. Conversely, it is worth noting that the use of NiTiNOL wires at the minimum pretension level allows to recover the equivalent damping ratio of the inflated beam once the internal pressure is equal to or larger than 0.10 bar. Increasing the pretension level of the metallic wires further reduces the equivalent damping ratio of the tensairity with respect to

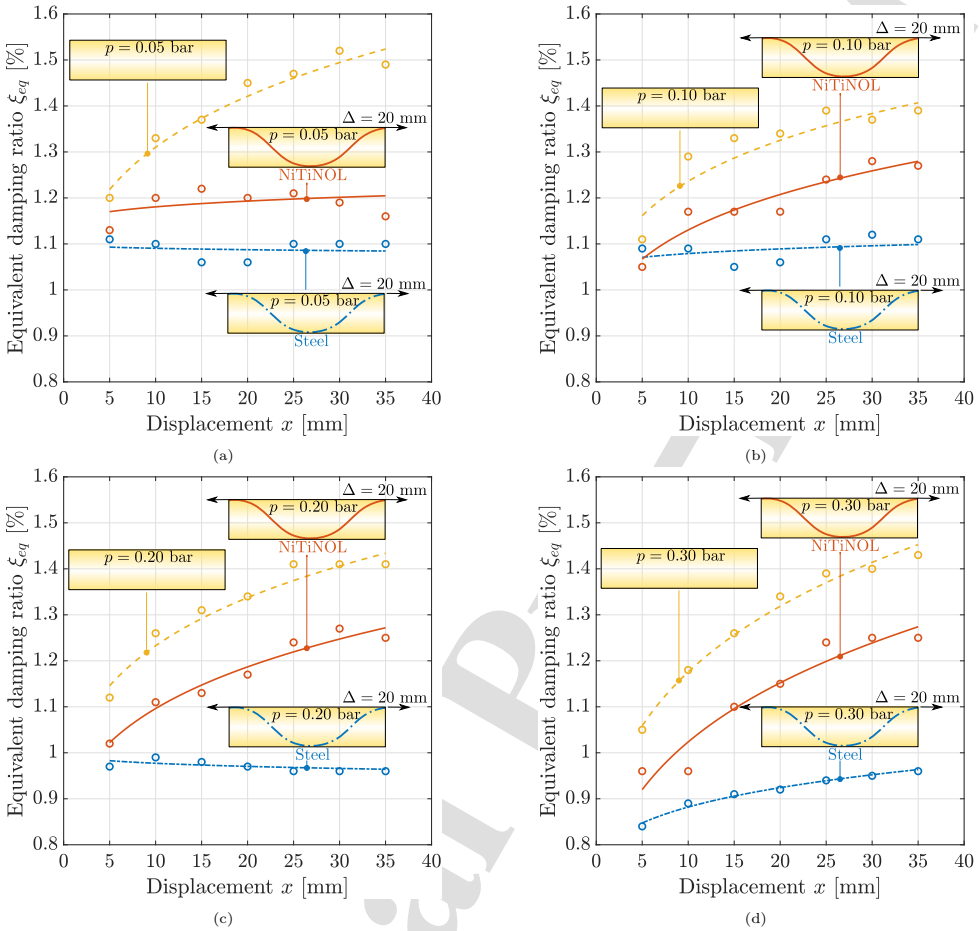

Figure 10: Equivalent damping ratio of the tensairity without cables and with metallic wires made of steel or NiTiNOL at the maximum pretension level of 20 mm: the internal pressure of the inflated beam is set to (a) 0.05 bar, (b) 0.10 bar, (c) 0.20 bar, and (d) 0.30 bar.

that of the standalone inflated beam. For the tensairity with steel wires under maximum pretension, the equivalent damping ratio turns out to be fairly constant and almost equal to 1.1% up to 0.10 bar while it falls below 1% for larger values of the internal pressure, even for the largest cyclic load corresponding to a displacement amplitude of 35 mm. The tensairity with NiTiNOL wires at the maximum pretension level exhibits a superior dissipation capacity especially for intermediate and large maximum displacements, being 1.2%-1.3% for the most severe cyclic loading condition.

The influence of the wires' material (i.e., steel vs. NiTiNOL) on the actual damping of the tensairity is also elucidated in Fig. 11. It shows the normalized equivalent damping ratio $\bar{\xi}_{eq}$, which is defined as the ratio between the equivalent damping ratio of the tensairity (with steel or NiTiNOL cables at both minimum and maximum pretension level) and the corresponding value of the standalone inflated beam for each maximum value of the imposed displacement throughout the cyclic loading.

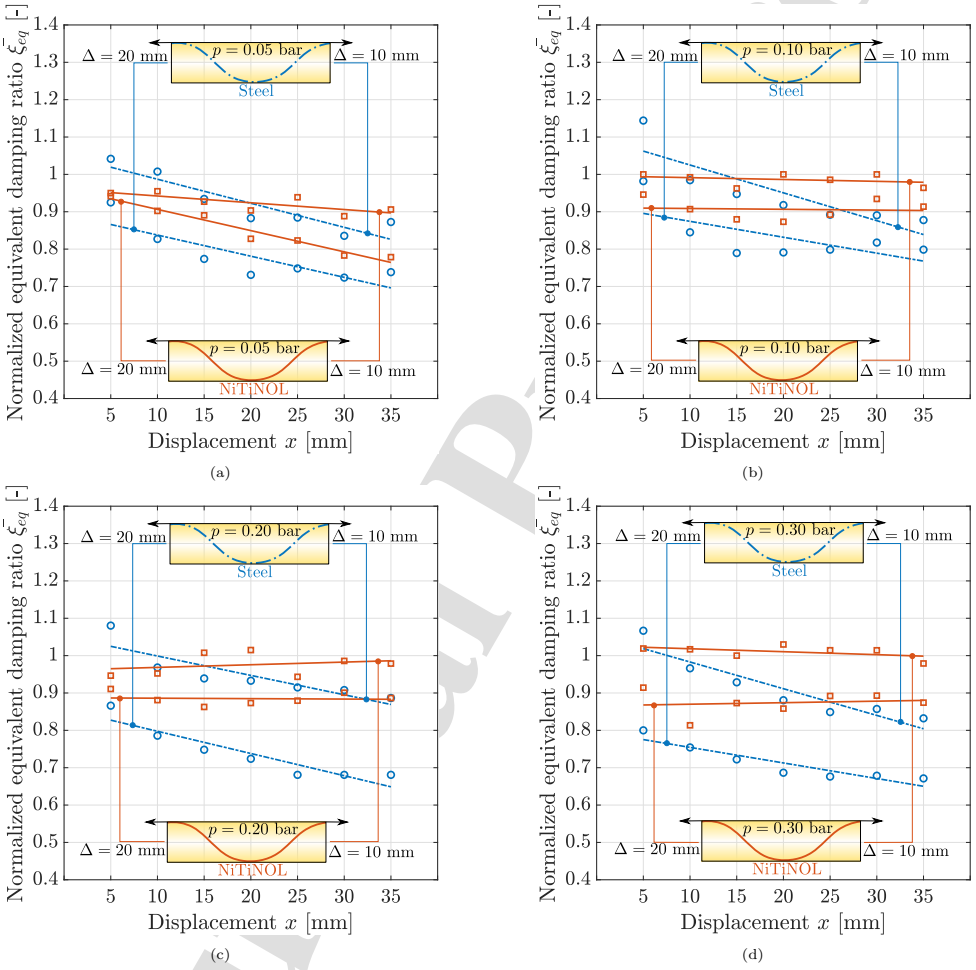

Figure 11: Equivalent damping ratio of the tensairity with metallic wires made of steel or NiTiNOL normalized with respect to the corresponding value estimated without cables: the internal pressure of the inflated beam is set to (a) 0.05 bar, (b) 0.10 bar, (c) 0.20 bar, and (d) 0.30 bar.

Figure 11 confirms the decreasing inherent dissipation capacity of the airbeam when enveloped by metallic wires. In the case of steel wires, the reduction is found to be proportional to the magnitude of the imposed displacement during cyclic loading, with a notable impact, especially in the case of the tensairity with steel wires at maximum pretension level. Here, a drastic reduction of almost 40% in the inherent dissipation capacity of the airbeam is observed at the maximum imposed displacement level for an internal pressure of 0.30 bar. The utilization of NiTiNOL wires markedly augments the dissipation capacity of the tensairity. With the potential exception of the airbeam inflated at the minimum pressure level, the tensairity with NiTiNOL wires at the minimum pretension level exhibits an equivalent damping ratio almost identical to the airbeam alone. Meanwhile, it decreases by no more than about 10% in the case of the maximum pretension level. Additionally, unlike the diminishing dissipation capacity observed with steel wires at larger displacement values, the use of NiTiNOL wires maintains an almost constant dissipation capacity in comparison to the airbeam alone. The reduction of damping capacity is due to the fact that the dissipated energy does not grow with the same rate as the stored energy when the cables are wrapped around the airbeam.

3.2. Phenomenological modeling

The modified Bouc-Wen model proposed by Carboni et al. [42] is here considered to describe the experimental hysteretic response under cyclic loading. This phenomenological model accounts for pinching through a suitable modification of the stiffness at the origin in the classic Bouc-Wen model. The restoring force is $f = k_e\, x + z$, where $k_e\, x$ is the linear elastic force and the hysteretic force z is expressed as follows:

$$\dot{z} = \left\{k_d h(x) - \left[\gamma + \beta \mathrm{sgn}\left(z\dot{x}\right)\right] |z|^n\right\} \dot{x}. \tag{2}$$

Herein, $k = k_e + k_d$ is the tangent stiffness at the origin. The model parameters γ and β rule the type of hysteresis (i.e., softening vs. hardening) whereas n regulates the smoothness of the transition from the elastic to the elasto-plastic behavior (i.e., the elasto-perfectly plastic behavior is recovered for $n \to \infty$). The bell-shaped function h:

$$h(x) = 1 - \zeta \mathrm{e}^{-x^2/x_d}. \tag{3}$$

serves the purpose of modifying the tangent stiffness in the neighborhood of the origin through two parameters, namely $\zeta \in [0, 1)$ and $x_d > 0$. The parametric identification of this phenomenological model is performed by searching for the set of parameters $\{k_e, k_d, \beta, \zeta, x_d\}$ that minimizes the mean square error

between the experimentally measured and numerically computed force, while the remaining parameters are set to $n = 1$ and $\gamma = 0$. The parametric identification problem is solved by means of the Differential Evolution algorithm [43, 44]. Experimental data for the airbeam only and those for the tensairity with steel or NiTiNOL cables at both pretension levels are considered.

The comparison between some measured and simulated force-displacement cycles is provided in Figs. 12-15. The identified model parameters are reported in Figs. 16-17. Figures 12-15 demonstrate that the modified Bouc-Wen model [42] can accurately reproduce most of the features of the experimental hysteretic behavior, including the observed pinching. It is evident in Figs. 12-15 that the model underestimates systematically the stiffness for low displacements while it is more accurate otherwise. Since the considered model does not take into account stiffness degradation effects, the parametric identification strives to look for the best trade-off across all displacement amplitudes. This, in turn, gets reflected into a more accurate description of the response at large displacements to minimize the overall error.

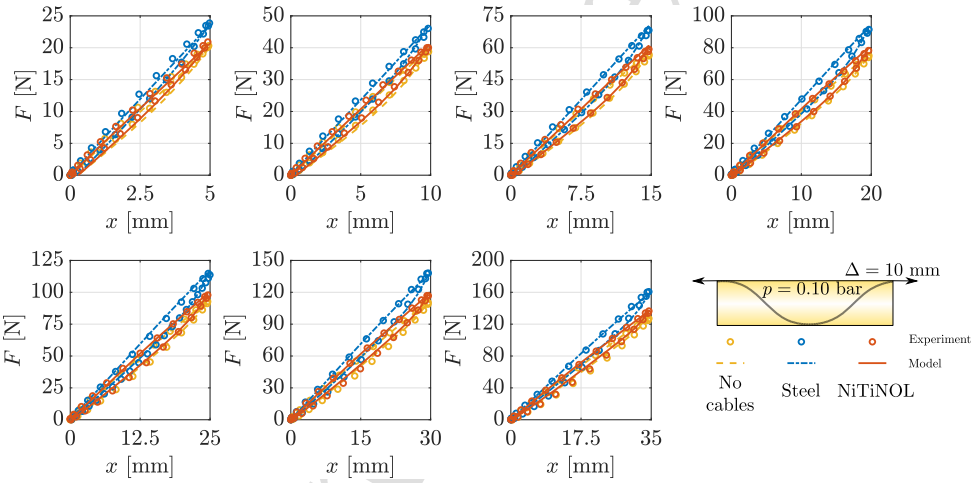

Figure 12: Comparison between experimental data and identified force-displacement cycles at the minimum pretension level for an internal pressure of the inflated beam equal to 0.10 bar.

The overall reliability of the assumed phenomenological model is based on its capacity to predict the structure's response under conditions beyond those employed in the parametric identification. Consequently, the estimated model parameters for internal pressures set to 0.05 bar, 0.10 bar, 0.20 bar, and 0.30 bar (see Tabs. 1-5) are utilized to predict the corresponding values at 0.15 bar and 0.25 bar through nonlinear regression methods. The predicted force-displacement cycles shown in Figs. 18-21 for such new conditions are once again in very good agreement with the experimental data. This evidence confirms that the parameters

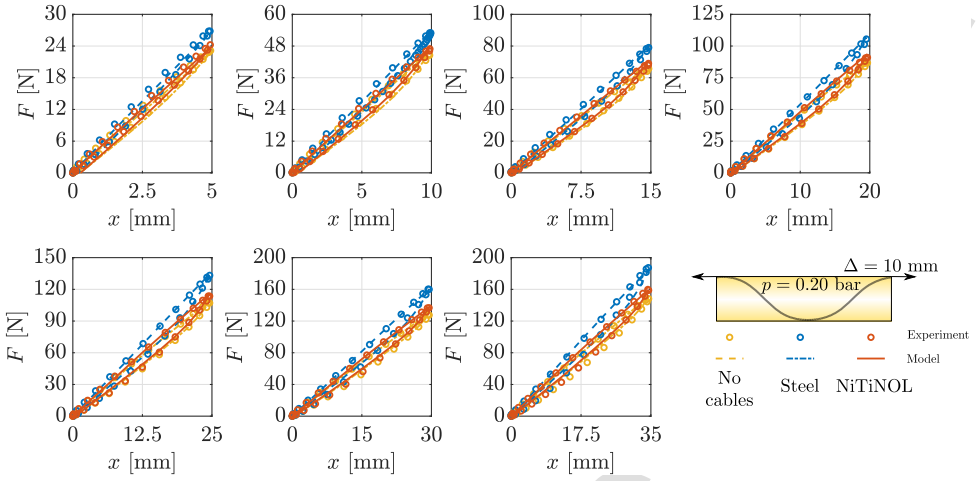

Figure 13: Comparison between experimental data and identified force-displacement cycles at the minimum pretension level for an internal pressure of the inflated beam equal to 0.20 bar.

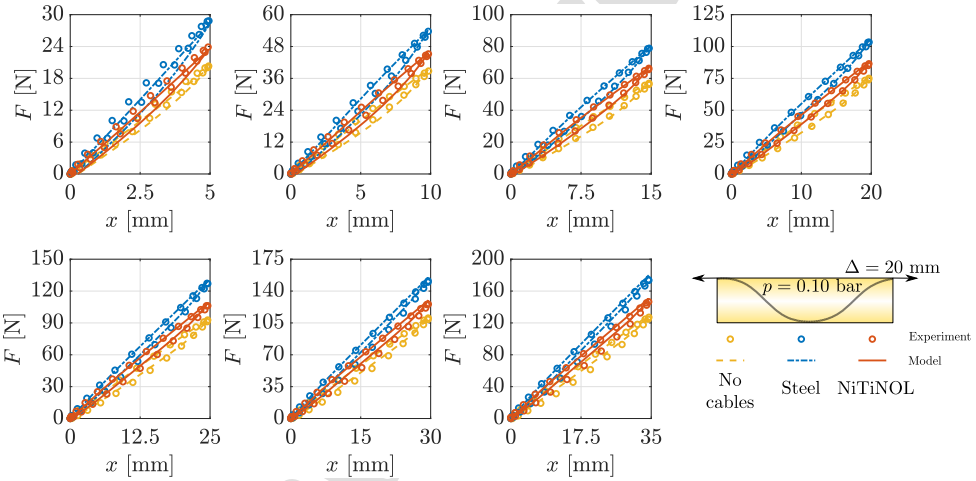

Figure 14: Comparison between experimental data and identified force-displacement cycles at the maximum pretension level for an internal pressure of the inflated beam equal to 0.10 bar.

of the considered phenomenological model can be conveniently related to the main features of the tensairity to perform sensitivity analyses at the preliminary stage of the design process.

p [bar]	k_e [kN/mm]	k_d [kN/mm]	β [kN^{1-n}/mm]	ζ [–]	x_d [mm^2]	MSE [%]
0.05	3.21×10^{-3}	1.54×10^{-3}	0.326	0.65	48.63	4.41
0.10	3.64×10^{-3}	2.06×10^{-3}	0.495	0.78	28.89	2.68
0.15	3.97×10^{-3}	2.49×10^{-3}	0.547	0.82	32.64	2.71
0.20	4.22×10^{-3}	2.60×10^{-3}	0.498	0.78	48.94	2.53
0.25	4.49×10^{-3}	2.56×10^{-3}	0.451	0.74	61.06	2.70
0.30	4.59×10^{-3}	2.64×10^{-3}	0.425	0.77	65.28	2.41

Table 1: Identified parameters of the modified Bouc-Wen model for the tensairity configuration without cables and associated mean square error (MSE).

p [bar]	k_e [kN/mm]	k_d [kN/mm]	β [kN^{1-n}/mm]	ζ [–]	x_d [mm^2]	MSE [%]
0.05	3.98×10^{-3}	2.97×10^{-3}	0.390	0.79	243.3	2.56
0.10	4.38×10^{-3}	2.96×10^{-3}	0.378	0.81	139.9	1.85
0.15	4.53×10^{-3}	3.18×10^{-3}	0.301	0.82	287.8	1.84
0.20	5.04×10^{-3}	3.88×10^{-3}	0.319	0.86	265.6	1.89
0.25	5.41×10^{-3}	3.35×10^{-3}	0.259	0.91	179.2	1.61
0.30	5.76×10^{-3}	3.96×10^{-3}	0.254	0.88	277.4	1.74

Table 2: Identified parameters of the modified Bouc-Wen model for the tensairity configuration equipped with steel cable at the minimum tensile stress and associated mean square error (MSE).

p [bar]	k_e [kN/mm]	k_d [kN/mm]	β [kN^{1-n}/mm]	ζ [–]	x_d [mm^2]	MSE [%]
0.05	4.69×10^{-3}	1.79×10^{-3}	0.506	0.73	10.61	2.97
0.10	5.11×10^{-3}	2.09×10^{-3}	0.520	0.74	11.00	3.60
0.15	5.99×10^{-3}	2.51×10^{-3}	0.612	0.77	14.34	1.88
0.20	6.42×10^{-3}	2.54×10^{-3}	0.567	0.72	22.42	1.94
0.25	6.69×10^{-3}	2.50×10^{-3}	0.567	0.86	9.74	2.06
0.30	7.16×10^{-3}	2.10×10^{-3}	0.377	0.77	10.83	2.58

Table 3: Identified parameters of the modified Bouc-Wen model for the tensairity configuration equipped with steel cable at the maximum tensile stress and associated mean square error (MSE).

p [bar]	k_e [kN/mm]	k_d [kN/mm]	β [kN^{1-n}/mm]	ζ [–]	x_d [mm^2]	MSE [%]
0.05	3.40×10^{-3}	2.16×10^{-3}	0.522	0.75	47.37	2.61
0.10	3.81×10^{-3}	2.44×10^{-3}	0.459	0.76	80.38	2.20
0.15	4.14×10^{-3}	2.72×10^{-3}	0.470	0.79	69.68	2.37
0.20	4.42×10^{-3}	2.93×10^{-3}	0.410	0.79	110.52	2.06
0.25	4.66×10^{-3}	3.22×10^{-3}	0.423	0.82	102.24	2.15
0.30	4.86×10^{-3}	3.21×10^{-3}	0.410	0.77	107.74	2.36

Table 4: Identified parameters of the modified Bouc-Wen model for the tensairity configuration equipped with NiTiNOL cable at the minimum tensile stress and associated mean square error (MSE).

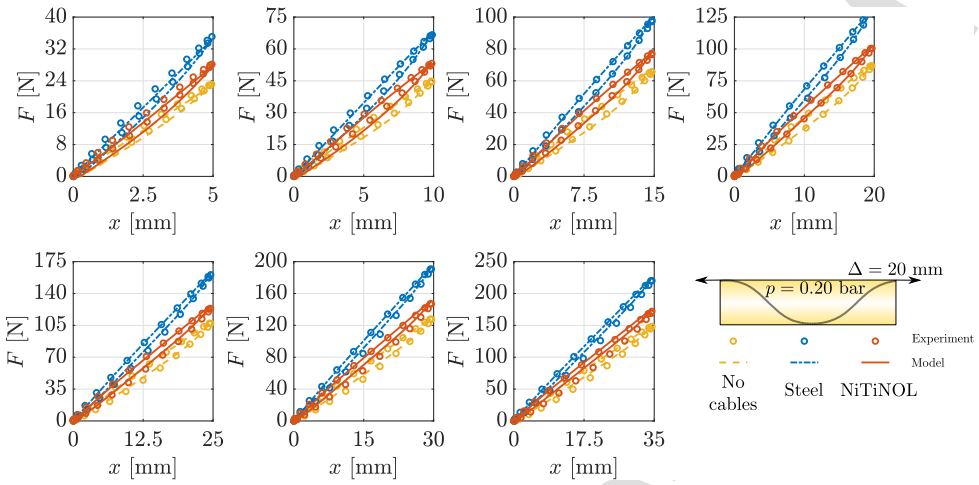

Figure 15: Comparison between experimental data and identified force-displacement cycles at the maximum pretension level for an internal pressure of the inflated beam equal to 0.20 bar.

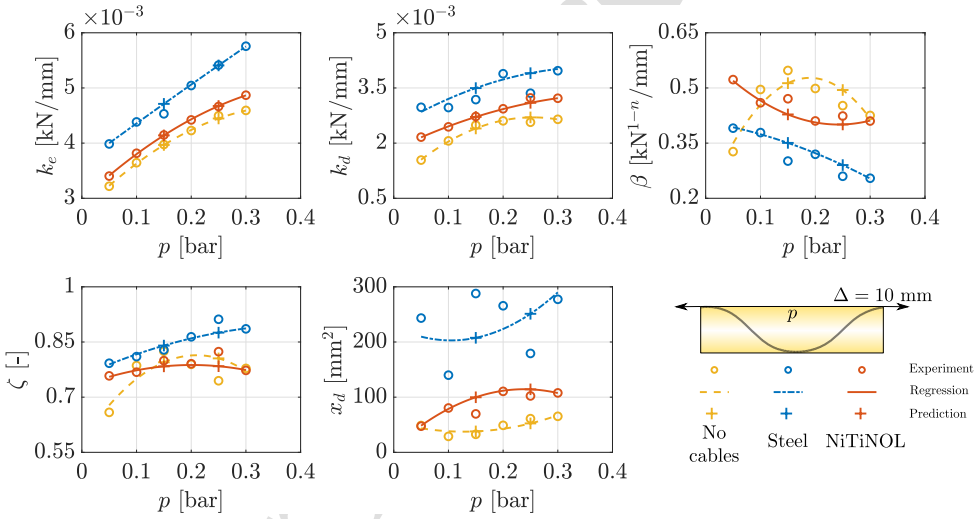

Figure 16: Identified model parameters at the minimum pretension level for different internal pressures of the inflated beam.

4. Conclusions

Tensairity structures offer a promising and feasible solution for numerous engineering applications. However, despite their robust load-bearing capacity under static loads, conventional pneumatic structures face limitations in managing dynamic loads due to their limited dissipation capacity. To overcome this drawback,

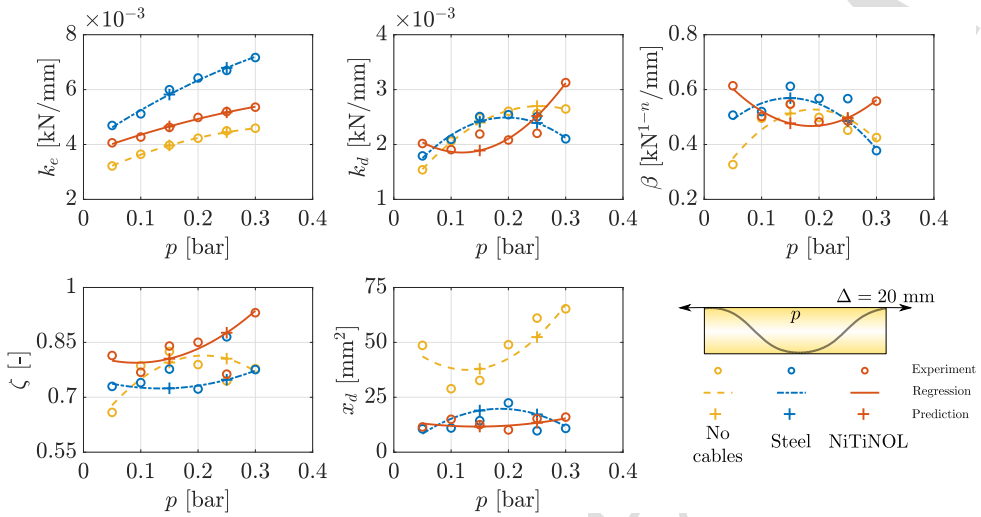

Figure 17: Identified model parameters at the maximum pretension level for different internal pressures of the inflated beam.

p [bar]	k_e [kN/mm]	k_d [kN/mm]	β [kN^{1-n}/mm]	ζ [–]	x_d [mm^2]	MSE [%]
0.05	4.06×10^{-3}	2.01×10^{-3}	0.613	0.814	11.48	3.24
0.10	4.27×10^{-3}	1.90×10^{-3}	0.502	0.768	14.96	3.38
0.15	4.62×10^{-3}	2.19×10^{-3}	0.547	0.840	12.52	3.52
0.20	4.98×10^{-3}	2.08×10^{-3}	0.482	0.850	10.14	3.79
0.25	5.20×10^{-3}	2.20×10^{-3}	0.485	0.763	15.25	3.31
0.30	5.36×10^{-3}	3.12×10^{-3}	0.558	0.931	15.97	1.12

Table 5: Identified parameters of the modified Bouc-Wen model for the tensairity configuration equipped with NITiNOL cable at the maximum tensile stress and associated mean square error (MSE).

a novel tensairity structure is explored, featuring NiTiNOL cables in lieu of traditional steel cables wrapped around the inflatable beam equipped with cable tension and pressure control units.

experimental tests on a laboratory-scale prototype have revealed that the tensairity with steel cables excels in stiffness and bearing capacity, but at the expense of a limited dissipation capacity. In contrast, the adoption of NiTiNOL cables enhances and preserves a consistent dissipation capacity, albeit with a trade-off of reduced stiffness and bearing capacity. Moreover, experimental tests have highlighted a softening-type hysteretic response under cyclic loading, accompanied by a minor decrease in stiffness and moderate pinching. Finally, numerical simulations have demonstrated that the observed hysteretic behavior can be accurately described and predicted using a simplified phenomenological model (e.g., a modified Bouc-Wen model for pinching hysteresis) after a thorough parametric identification process. This research lays the foundation for a more adaptable design of tensairity structures, enabling optimization and customization efforts to meet

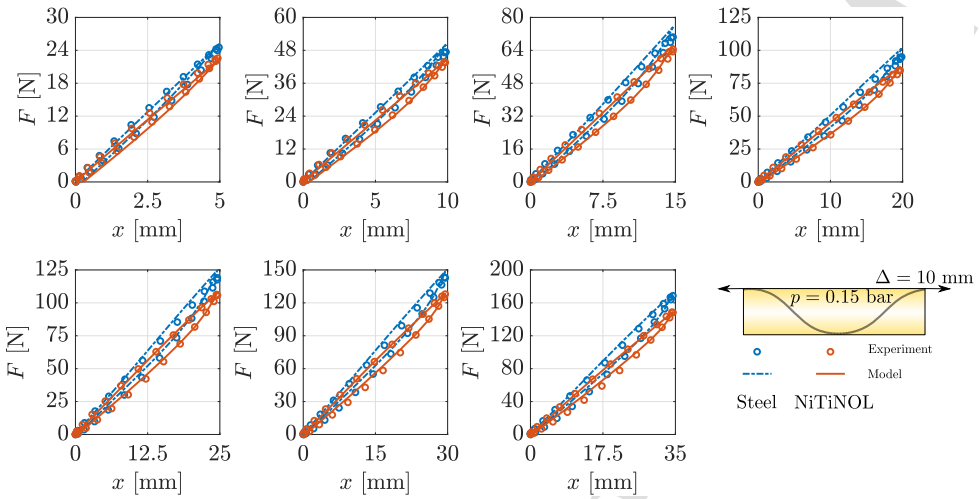

Figure 18: Comparison between experimental data and simulated force-displacement cycles with predicted model parameters at the minimum pretension level for an internal pressure of the inflated beam equal to 0.15 bar.

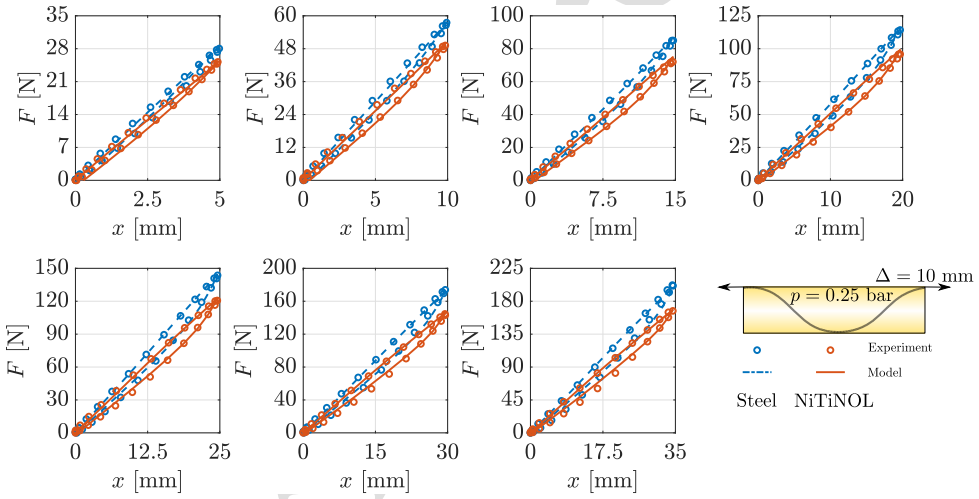

Figure 19: Comparison between experimental data and simulated force-displacement cycles with predicted model parameters at the minimum pretension level for an internal pressure of the inflated beam equal to 0.25 bar.

the diverse needs of various applications in civil and aerospace engineering.

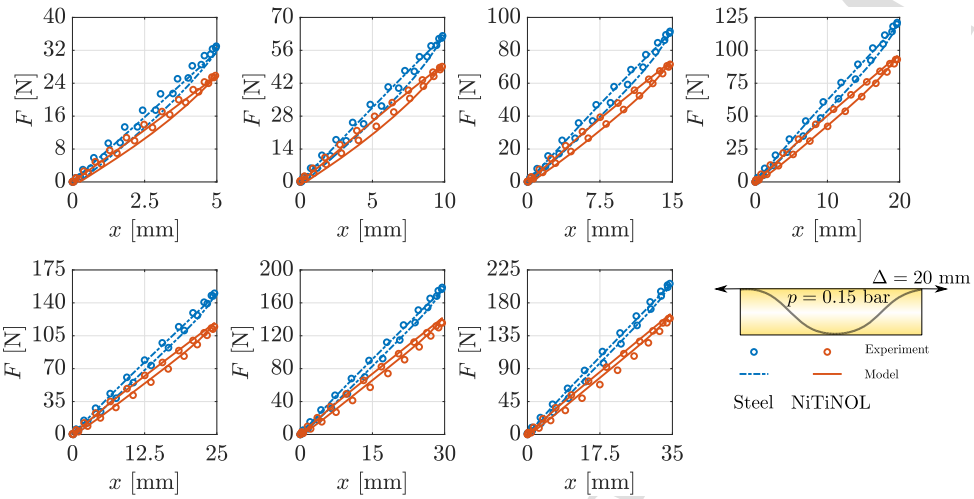

Figure 20: Comparison between experimental data and simulated force-displacement cycles with predicted model parameters at the maximum pretension level for an internal pressure of the inflated beam equal to 0.15 bar.

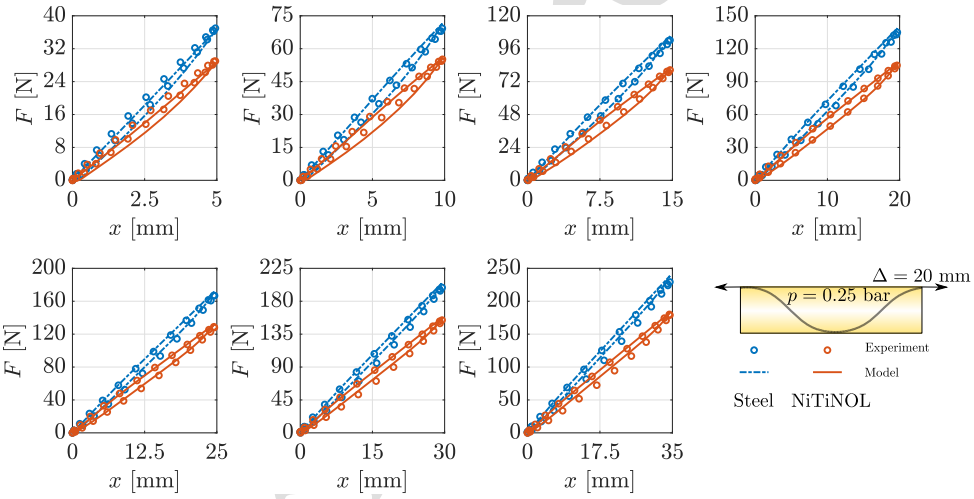

Figure 21: Comparison between experimental data and simulated force-displacement cycles with predicted model parameters at the maximum pretension level for an internal pressure of the inflated beam equal to 0.25 bar.

Acknowledgments

This work was supported by the Ministry of Enterprises and Made in Italy and Sapienza University of Rome under the program 'BIT4MaPS 2019-2021', GRANT 'Tensair' (PI: W. Lacarbonara, CUP:

C82C20003940006). It is partially supported under GRANT RM1221816C52B759, 'Progetti Medi 2021' (PI: B. Carboni) and Project ECS 0000024 Rome Technopole, CUP B83C22002820006, National Recovery and Resilience Plan (NRRP) Mission 4 Component 2 Investment 1.5, funded by the European Union – NextGenerationEU.

Data availability statement

The data supporting the findings of this study are available upon reasonable request.

References

References

[1] H. Altenbach, "Mechanics of advanced materials for lightweight structures," *Proceedings of the Institution of Mechanical Engineers, Part C: Journal of Mechanical Engineering Science*, vol. 225, no. 11, pp. 2481–2496, 2011.

[2] J. Plocher and A. Panesar, "Review on design and structural optimisation in additive manufacturing: Towards next-generation lightweight structures," *Materials & Design*, vol. 183, p. 108164, 2019.

[3] R. M. D. O. Pauletti, "Some issues on the design and analysis of pneumatic structures," *International Journal of Structural Engineering*, vol. 1, no. 3-4, pp. 217–240, 2010.

[4] F. W. Lanchester, "Construction of tents for field-hospitals, depots, and like purposes," 1919. US Patent 1,302,182,182.

[5] W. W. Bird and M. Kamrass, *Design manual for spherical air supported radomes*. Cornell Aeronautical Laboratory, 1956.

[6] S. Veldman and C. Vermeeren, "Inflatable structures in aerospace engineering-an overview," *Spacecraft Structures, Materials and Mechanical Testing*, vol. 468, p. 93, 2001.

[7] R. Comer and S. Levy, "Deflections of an inflated circular-cylindrical cantilever beam," *AIAA journal*, vol. 1, no. 7, pp. 1652–1655, 1963.

[8] A. Topping, "Shear deflections and buckling characteristics of inflated members," *Journal of Aircraft*, vol. 1, no. 5, pp. 289–292, 1964.

[9] W. J. Douglas, "Bending stiffness of an inflated cylindrical cantilever beam.," *Aiaa Journal*, vol. 7, no. 7, pp. 1248–1253, 1969.

[10] H. Harrison, "The analysis and behaviuor of inflatable membrane dams under static loading.," *Proceedings of the Institution of Civil Engineers*, vol. 45, no. 4, pp. 661–676, 1970.

[11] J. Main, S. Peterson, and A. Strauss, "Load-deflection behavior of space-based inflatable fabric beams," *Journal of Aerospace Engineering*, vol. 7, no. 2, pp. 225–238, 1994.

[12] C. Wielgosz and J.-C. Thomas, "Deflections of inflatable fabric panels at high pressure," *Thin-walled structures*, vol. 40, no. 6, pp. 523–536, 2002.

[13] C. Wang and H. Tan, "Experimental and numerical studies on wrinkling control of an inflated beam using sma wires," *Smart Materials and Structures*, vol. 19, no. 10, p. 105019, 2010.

[14] K. E. Brayley, W. G. Davids, and J. D. Clapp, "Bending response of externally reinforced, inflated, braided fabric arches and beams," *Construction and Building Materials*, vol. 30, pp. 50–58, 2012.

[15] J.-C. Thomas and A. Bloch, "Non linear behaviour of an inflatable beam and limit states," *Procedia Engineering*, vol. 155, pp. 398–406, 2016.

[16] K. N. Slade, M. L. Tinker, J. O. Lassiter, and R. Engberg, "Dynamics of an inflatable structure in vacuum and ambient conditions," *AIAA journal*, vol. 39, no. 5, pp. 894–901, 2001.

[17] G. Park, E. Ruggiero, and D. J. Inman, "Dynamic testing of inflatable structures using smart materials," *Smart Materials and Structures*, vol. 11, no. 1, p. 147, 2002.

[18] G. Park, M. Sausse, D. J. Inman, and J. A. Main, "Vibration testing and finite element analysis of an inflatable structure," *AIAA journal*, vol. 41, no. 8, pp. 1556–1563, 2003.

[19] J.-S. Lew, L. G. Horta, and M. C. Reaves, "Uncertainty quantification of an inflatable/rigidizable torus," *Journal of sound and vibration*, vol. 294, no. 3, pp. 615–623, 2006.

[20] R. Luchsinger, A. Pedretti, P. Steingruber, and M. Pedretti, "The new structural concept tensairity: Basic principles," *Progress in structural engineering, mechanics and computation*, pp. 323–328, 2004.

[21] R. H. Luchsinger and C. Galliot, "Structural behavior of symmetric spindle-shaped tensairity girders," *Journal of Structural Engineering*, vol. 139, no. 2, pp. 169–179, 2013.

[22] R. H. Luchsinger, A. Sydow, and R. Crettol, "Structural behavior of asymmetric spindle-shaped tensairity girders under bending loads," *Thin-walled structures*, vol. 49, no. 9, pp. 1045–1053, 2011.

[23] T. S. Plagianakos, U. Teutsch, R. Crettol, and R. H. Luchsinger, "Static response of a spindle-shaped tensairity column to axial compression," *Engineering Structures*, vol. 31, no. 8, pp. 1822–1831, 2009.

[24] T. E. Wever, T. S. Plagianakos, R. H. Luchsinger, and P. Marti, "Effect of fabric webs on the static response of spindle-shaped tensairity columns," *Journal of Structural Engineering*, vol. 136, no. 4, pp. 410–418, 2010.

[25] C. Galliot and R. H. Luchsinger, "Structural behavior of symmetric spindle-shaped tensairity girders with reinforced chord coupling," *Engineering Structures*, vol. 56, pp. 407–416, 2013.

[26] J. Roekens, L. De Laet, M. Mollaert, and R. Luchsinger, "Experimental and numerical investigation of a tensairity arch," *Thin-Walled Structures*, vol. 105, pp. 112–120, 2016.

[27] L. Lv, Z. Fan, and H. Sun, "Experimental study on bearing capacity of a tensairity arch," in *Journal of Physics: Conference Series*, vol. 2285, p. 012026, IOP Publishing, 2022.

[28] Z. Cao, Z. Wan, Y. Sun, and F. Fan, "Numerical simulation study on structural behavior of tensairity domes with annular airbags," *Thin-Walled Structures*, vol. 117, pp. 155–164, 2017.

[29] Z. Wan, Z. Cao, Y. Sun, and F. Fan, "Pre-stressing method and structural behaviour of a tensairity dome with multiple inflated cushions," *Thin-Walled Structures*, vol. 132, pp. 585–595, 2018.

[30] Z. Wan, Z. Cao, Y. Sun, and F. Fan, "Experimental and numerical research on the structural behaviour of a tensairity dome," *Engineering Structures*, vol. 248, p. 113225, 2021.

[31] P. Vernarsky, M. Tomko, R. Soltys, and S. Kmet, "Numerical simulations of wind circumfluence around a tensairity cylindrical beam and predictions of its response," *Advances in Engineering Software*, vol. 129, pp. 13–34, 2019.

[32] R. Klis, E. Chatzi, C. Galliot, R. Luchsinger, and G. Feltrin, "Modal identification and dynamic response assessment of a tensairity girder," *Journal of Structural Engineering*, vol. 143, no. 2, p. 04016165, 2017.

[33] R. H. Luchsinger and R. Crettol, "Experimental and numerical study of spindle shaped tensairity girders," *International journal of space structures*, vol. 21, no. 3, pp. 119–130, 2006.

[34] C. Galliot and R. Luchsinger, "Non-linear properties of pvc-coated fabrics used in tensairity structures," in *17th Interna-*

tional Conference on Composite Materials, 2009.

[35] P. Beccarelli, R. Maffei, C. Galliot, and R. H. Luchsinger, "A new generation of temporary pavilions based on tensairity girders," *Steel Construction*, vol. 8, no. 4, pp. 259–264, 2015.

[36] J. C. Breuer and R. H. Luchsinger, "Inflatable kites using the concept of tensairity," *Aerospace Science and Technology*, vol. 14, no. 8, pp. 557–563, 2010.

[37] Z. Cao, Z. Wan, J. Yan, and F. Fan, "Static behaviour and simplified design method of a tensairity truss with a spindle-shaped airbeam," *Journal of Constructional Steel Research*, vol. 145, pp. 244–253, 2018.

[38] T. Griffith and J. A. Main, "Modal testing of an inflated thin film polyimide torus structure# 69," in *Proceedings of IMAC-XVIII: A Conference on Structural Dynamics*, vol. 4062, p. 1035, 2000.

[39] K. Ke, H. Zhang, X. Zhou, M. C. Yam, Y. Wang, and T. Shi, "Hybrid-self-centring steel frames: Insights and probabilistic seismic assessment," *Engineering Structures*, vol. 303, p. 117516, 2024.

[40] X. Zhou, Y. Huang, K. Ke, M. C. Yam, H. Zhang, and H. Fang, "Large-size shape memory alloy plates subjected to cyclic tension: Towards novel self-centring connections in steel frames," *Thin-Walled Structures*, vol. 185, p. 110591, 2023.

[41] K. Ke, X. Zhou, M. Zhu, M. C. Yam, and H. Zhang, "Seismic demand amplification of steel frames with smas induced by earthquake sequences," *Journal of Constructional Steel Research*, vol. 207, p. 107929, 2023.

[42] B. Carboni, W. Lacarbonara, and F. Auricchio, "Hysteresis of multiconfiguration assemblies of nitinol and steel strands: experiments and phenomenological identification," *Journal of Engineering Mechanics*, vol. 141, no. 3, p. 04014135, 2015.

[43] R. Storn and K. Price, "Differential evolution–a simple and efficient heuristic for global optimization over continuous spaces," *Journal of global optimization*, vol. 11, pp. 341–359, 1997.

[44] G. Quaranta, W. Lacarbonara, and S. F. Masri, "A review on computational intelligence for identification of nonlinear dynamical systems," *Nonlinear Dynamics*, vol. 99, no. 2, pp. 1709–1761, 2020.

Highlights

- Tensairity is a formidable structure characterized by lightness, portability, ease of installation, and high static loading capacity compared to its self-weight.
- The possibility to increase the structural damping for tensairities allows for their application in situations where dynamic loads must be considered.
- The utilization of shape memory cables can significantly enhance the dissipation capacity of tensairity structures.
- Tensairity structures can be employed in various applications, including long-span roofs, temporary bridges, aerostats, dirigibles, stratospheric platforms, and space habitats.

Stefano Catarci: Methodology, Software, Validation, Investigation, Data Curation, Writing - Original Draft, Writing - Review & Editing. **Sawan Kumar Guruva:** Methodology, Software, Validation, Investigation, Data Curation, Writing - Review & Editing. **Biagio Carboni:** Conceptualization, Methodology, Formal analysis, Data Curation, Writing - Original Draft, Writing - Review & Editing, Supervision, Project administration, Funding acquisition. **Giuseppe Quaranta:** Conceptualization, Methodology, Formal analysis, Data Curation, Visualization, Writing - Original Draft, Writing - Review & Editing, Supervision, Project administration, Funding acquisition. **Walter Lacarbonara**: Conceptualization, Methodology, Formal analysis, Writing - Original Draft, Writing - Review & Editing, Supervision, Project administration, Funding acquisition.

Declaration of interests

☐ The authors declare that they have no known competing financial interests or personal relationships that could have appeared to influence the work reported in this paper.

☒ The authors declare the following financial interests/personal relationships which may be considered as potential competing interests:

Biagio Carboni reports financial support was provided by University of Rome La Sapienza. Biagio Carboni reports financial support was provided by Ministry of Enterprises and Made in Italy. Biagio Carboni reports financial support was provided by European Union. Walter Lacarbonara reports financial support was provided by University of Rome La Sapienza. Walter Lacarbonara reports financial support was provided by Ministry of Enterprises and Made in Italy. Walter Lacarbonara reports financial support was provided by European Union. Giuseppe Quaranta reports financial support was provided by University of Rome La Sapienza. Giuseppe Quaranta reports financial support was provided by Ministry of Enterprises and Made in Italy. Giuseppe Quaranta reports financial support was provided by European Union. Stefano Catarci reports financial support was provided by University of Rome La Sapienza. Sawan Kumar Guruva reports financial support was provided by University of Rome La Sapienza. Sawan Kumar Guruva reports financial support was provided by Ministry of Enterprises and Made in Italy. Walter Lacarbonara has patent "Tensairity structure with shape memory alloy" pending to US15/756,585, EP16801320.9A, CN201680055349.2A. Biagio Carboni has patent "Tensairity structure with shape memory alloy" pending to US15/756,585, EP16801320.9A, CN201680055349.2A. If there are other authors, they declare that they have no known competing financial interests or personal relationships that could have appeared to influence the work reported in this paper.